CMS Physics Analysis Summary

New constraints of initial states in PbPb collisions with Z boson yields and azimuthal anisotropy at $\sqrt{s_{\mathrm{NN}}} = 5.02$ TeV

The CMS Collaboration

Abstract

The differential yields of Z bosons decaying to a pair of leptons are measured in PbPb collisions collected by the CMS experiment at the LHC. The measurements are performed for collisions at 5.02 TeV, using both the muon and electron decay channels. The yields in various centrality bins are compared to Glauber model predictions of the production rates of hard probes not modified by the presence of a hot medium. For the first time, Z boson yields in peripheral collisions are found to deviate from the canonical scaling expected for colorless hard probes, indicating the presence of initial collision geometry and centrality selection biases. Because the measurement uncertainties are comparable to the uncertainties of a Glauber-scaled reference, Z boson yields can now be used as an experimental measure of the effective nucleon-nucleon luminosity without loss of precision. A high precision measurement of the Z boson azimuthal anisotropy (v_2) is also found to be compatible with zero, showing that Z bosons do not experience significant final-state modification in heavy ion collisions.

In high energy heavy ion collisions, a hot medium known as the quark-gluon plasma (QGP) can cause high-energy partons to lose energy. This is known as "jet quenching" [1, 2]. The strength of quenching is frequently quantified using the nuclear modification factor [2]. To have a meaningful physical interpretation, this observable assumes that the production rate of hard processes scales with the number of binary nucleon-nucleon collisions (N_{coll}) present in a collision with a given initial geometry. The Monte Carlo (MC) Glauber model is typically used to calculate N_{coll} as a function of impact parameter (or "centrality") [3].

The Z boson has a relatively large mass and decays before the QGP has a sufficient time to cause quenching effects. Additionally, Z bosons and their leptonic daughters carry no color charge and are not expected to interact strongly with the QGP medium. Thus, they provide a clean probe of the N_{coll} scaling assumption [4–6] because they are not strongly affected by final-state effects. Previous measurements by the ATLAS, ALICE, and CMS Collaborations found that Z boson yields were consistent with the MC Glauber model expectation [4–7]. Measurements of W bosons [8, 9] and direct photons [10–12] have also found similar results. However, these studies were statistically limited for glancing, or "peripheral," collisions. In measurements of nuclear modification factors for colored hard probes such as charged hadrons, jets, and quarkonia, significant apparent suppression persists in even very peripheral events, presenting a challenge to theoretical interpretations. In this region, the Glauber model has large uncertainties in determining N_{coll}. Thus, understanding the onset of jet quenching from peripheral to central events remains a key open question in the field. Furthermore, the discovery of QGP-like behavior in small-system collisions (e.g, pp, pPb) [13, 14] indicates the possibility of final-state effects that may also lead to jet quenching. Current efforts in searching for quenching in small systems are hindered by uncertainties in N_{coll}. A high precision measurement of Z boson yield in the peripheral region will provide a data-driven reference to hard probes in absence of final-state effects, which may lead to a breakthrough in understanding the onset of jet quenching in peripheral and/or small-system collisions.

In this note, the yields of Z bosons decaying to a pair of electrons or muons are measured using the 2018 dataset of PbPb collisions recorded by CMS at $\sqrt{s_{NN}}$ = 5.02 TeV, and compared to Glauber model predictions for N_{coll} scaling of hard, colorless probes. A precision measurement of the Z boson elliptic azimuthal anisotropy coefficient (v_2) is also presented. The v_2 is defined as $\langle \cos[2(\phi_Z - \Psi_2)] \rangle$, where ϕ_Z is a Z boson's azimuthal angle and Ψ_2 is the angle of maximum azimuthal particle density [15]. Finally, the Z boson transverse momentum (p_T) and rapidity (y) distributions are examined. The contribution of virtual photon production ($\gamma^* \to \ell^+ \ell^-$) is included in the Z boson signal in this work.

The central feature of the CMS apparatus is a superconducting solenoid of 6 m internal diameter, providing a magnetic field of 3.8 T. Within the solenoid volume are a silicon pixel and strip tracker, a lead tungstate crystal electromagnetic calorimeter (ECAL), and a brass and scintillator hadron calorimeter (HCAL), each composed of a barrel and two endcap sections. Forward (HF) calorimeters extend the pseudorapidity coverage provided by the barrel and endcap detectors. Muons are detected in gas-ionization chambers embedded in the steel flux-return yoke outside the solenoid. Events of interest are selected using a two-tiered trigger system [16]. A more detailed description of the CMS detector, together with a definition of the coordinate system used and the relevant kinematic variables, can be found in Ref. [17].

The dataset in this analysis corresponds to an integrated luminosity of 1.696 ± 0.032 nb^{-1}. Events containing at least one muon (electron) with $p_T > 12$ GeV (20 GeV) are selected by the trigger system. Each event must have at least one reconstructed primary vertex. The data is filtered to remove background contributions such as cosmic-ray muons and beam-gas inter-

Table 1: T_{AA} values for $\sqrt{s_{NN}} = 5.02$ TeV PbPb collisions. The uncertainties result from uncertainties in the model parameters and the HF detector energy resolution.

Centrality	T_{AA} [mb^{-1}]	Centrality	T_{AA} [mb^{-1}]
0–5%	25.70 ± 0.47	40–50%	2.78 ± 0.11
5–10%	20.40 ± 0.40	50–70%	0.996 ± 0.050
10–20%	14.39 ± 0.30	70–90%	0.1650 ± 0.0077
20–30%	8.80 ± 0.22	0–90%	6.27 ± 0.14
30–40%	5.12 ± 0.16	0–100%	5.65 ± 0.12

actions. Collision centrality is determined from the total transverse energy deposited in both HF calorimeters. The centrality is expressed as a percentage of the total hadronic cross section, with the 0–5% range corresponding to head-on (central) collisions and 70–90% for peripheral collisions. After these selections the dataset corresponds to an effective number of sampled minimum-bias (MB) events (N_{MB}) of $11.54 \pm 0.14 \times 10^9$ in the 0–90% range.

Central collisions involve a larger number of binary nucleon-nucleon collisions than peripheral events, resulting in more hard scatterings. The nuclear overlap function, T_{AA}, is a measure of the average effective nucleon-nucleon luminosity delivered by a single heavy ion collision at a given centrality [3] and can be used to normalize different centrality selections for a direct comparison. It is calculated using the Glauber model [3], as implemented in the TGLAUBERMC v3.2 software package [18]. The T_{AA} values used in this analysis are given in Table 1. The total hadronic PbPb cross section (σ_{MB}^{PbPb}) is 7.644 ± 0.008 b in this model.

Simulated Monte Carlo (MC) events are used to study detector performance. The signal sample consists of Drell-Yan production ($Z/\gamma^* \to \ell^+\ell^-$) generated with MADGRAPH5_AMC@NLO (v2.4.2) at next-to-leading order (NLO) [19]. Up to two extra partons are included at the matrix-element (ME) level. The FXFX merging procedure is employed to prevent double counting of partons [20]. The same generator and settings are used to model the production of background $t\bar{t}$ and W boson production. Simulations account for the isospin content of the lead nuclei and use the EPPS16 NLO nuclear parton distribution function (nPDF) [21] applied on top of the free-nucleon CT14 NLO PDF [22]. The ME level events are interfaced with the PYTHIA 8 (v2.3.0) generator [23, 24] to simulate parton showering, hadronization, and underlying event production using the "CMS PYTHIA8 CP5" tune [25]. These processes are then overlaid onto a heavy ion event produced with the HYDJET v1.9 event generator [26]. The final generated events are input into the GEANT4 [27] program to emulate detector response. The MC samples are weighted to reproduce the z position of the primary vertex, the centrality distribution, and the p_T spectrum of Z boson candidates seen in data.

Leptons are reconstructed using the CMS particle flow algorithm [28] and are not required to be isolated. Muon (electron) candidates must have $|\eta| < 2.4$ (2.1) and $p_T > 20$ GeV. A series of selection criteria are applied to reject poor quality muons [29], resulting in an identification efficiency of $\approx 98\%$. The effects of misreconstructed muons are negligible. The selection criteria applied to electrons [30] were optimized using the TMVA software package [31]. A working point corresponding to a 90% identification efficiency and 80% rejection of misreconstructed electrons is used. The efficiencies of various stages of the lepton reconstruction are measured using the tag-and-probe method [32] in both data and MC as a function of lepton p_T, η, and event centrality. This includes lepton trigger efficiency, the efficiency of reconstructing a muon (electron) track that matches a muon station (ECAL tower), and the probability that the lepton candidate passes all selection criteria. Discrepancies between data and MC are corrected by weighting the MC leptons by the ratio of the data to the MC efficiencies. The electron energy scale is systematically overestimated in central events because of underlying event contribu-

tions. A data-driven residual calibration is applied by scaling the electron energy by a constant factor to recenter the Z mass peak at its accepted value [30, 33].

Z boson candidates are constructed by forming pairs of oppositely-charged leptons having an invariant mass within $60 < m_{\ell\ell} < 120$ GeV and rapidity $|y| < 2.1$. This results in 19104 (9863) opposite-sign pairs in the muon (electron) channel. Applying the same procedure for same-sign lepton pairs results in 44 (167) dimuon (dielectron) candidates.

The Z boson reconstruction efficiency (ϵ) is calculated using a signal MC sample as a function of the Z p_T, y, and event centrality. The overall efficiency is around 70 to 95% (30 to 65%) from central to peripheral events in the dimuon (dielectron) channel. Candidates are weighted by $1/\epsilon$ to correct for lepton quality selection and detector inefficiencies. A similar correction for detector acceptance is applied to account for Z bosons having rapidity $|y| < 2.1$ with daughters outside the lepton p_T or η selections. The average acceptance is 0.68 (0.58) in the dimuon (dielectron) channel.

Multiple backgrounds can create a pair of high-mass leptons. The first is from quantum chromodynamics (QCD) initiated hard processes, such as the production of two leptons inside of jets. Because this background arises largely from random lepton combinations, it is assumed that the production rates of same-sign and opposite-sign lepton pairs are equal. In the electron channel, misreconstruction of an electron's charge results in a small enhancement of the same-sign yield. After correcting for this effect, this background is 0.2% (1.0%) of the total opposite sign yield in the dimuon (dielectron) channel.

A second background results from electromagnetic (EM) processes (e.g., $\gamma\gamma \to \ell^+\ell^-$). Here, the photons are emitted by the incoming nuclei and tend to have very low p_T [34]. Thus, the lepton pair p_T is strongly peaked near zero, and the daughter leptons are back-to-back in azimuth. Based on studies using STARLIGHT v2.2 [35] events, the dimuon (dielectron) candidates that have $p_T < 1.25$ GeV (2.5 GeV) and acoplanarity, defined as $A_\phi = 1 - \Delta\phi/\pi$, less than 0.001, are identified as products of EM backgrounds. The p_T threshold for the dielectron channel is larger because of the worse energy resolution of electrons compared to muons. These selections correspond to 90% background rejection, and result in a small efficiency loss for legitimate Z bosons, which is accounted for using the efficiency correction. Candidates identified as resulting from this background account for 0.6% (0.7%) of the dimuon (dielectron) yield before subtraction.

The other backgrounds considered are $Z \to \tau^+\tau^-$, $t\bar{t}$ production, and the production of W bosons decaying to a single lepton that is combined with another random lepton. For these three backgrounds, the expected yield is calculated as a function of centrality, Z boson p_T, or y using appropriate MC samples. These backgrounds are less than 0.3% contributions to the total yield.

The Z boson p_T resolution is around 6.5% (7.7)% in the dimuon (dielectron) channel. When measuring the Z p_T spectrum, this finite resolution results in the migration of Z candidates between bins. This is corrected using a matrix inversion unfolding procedure, as implemented by the RooUnfold framework [36]. The statistical uncertainty of the MC response matrix is propagated to the final spectrum as a systematic uncertainty. This uncertainty is up to 2% (4%) for the dimuon (dielectron) channel in the lowest p_T bin, but is less than 1% (2%) at higher p_T.

To measure the azimuthal anisotropy coefficient v_2, the 3-subevent scalar product method is used [15, 37]. In this method, the Z candidate Q-vector (defined as $e^{i2\phi_Z}$) is compared against a

reference Q-vector using the equation

$$v_2 = \frac{\langle Q_Z Q_A^* \rangle}{\sqrt{\frac{\langle Q_A Q_B^* \rangle \langle Q_A Q_C^* \rangle}{\langle Q_B Q_C^* \rangle}}}. \tag{1}$$

Here, Q_A and Q_B are measured using the HF calorimeters, and Q_C is determined using tracks having $|\eta| < 0.75$. A pseudorapidity gap of at least 3 units is required between the candidate and the Q_A reference calorimeter. Detector inefficiencies and acceptance are accounted for by recentering the reference Q-vectors [38, 39].

The centrality calibration is affected by the MB event selection efficiency of the HF calorimeters, which is $(97.5^{+1.0}_{-0.5})$% for the 0–100% centrality range. The uncertainty in this efficiency is propagated to the final results, resulting in a final uncertainty of 0.1% (8.4%) in central (peripheral) events.

The single lepton reconstruction efficiencies have uncertainties calculated from the tag-and-probe procedure. After accounting for each daughter of the Z boson decay, this uncertainty is 3.0% (5.9%) in the dimuon (dielectron) channel. A small additional uncertainty of less than 1% is included to account for the statistical uncertainty of the MC sample used to calculate the Z boson efficiency. The model dependence of the acceptance correction is calculated to be 0.6% by examining the impact of using different nPDF Hessian error sets [40].

The effect of electron charge misreconstruction is 0.5% in MC. Differences between the charge swapping probability in data and MC are estimated to be less than a factor of two, so an absolute uncertainty of 0.5% is quoted for this effect.

The A_ϕ and p_T selection criteria used to remove EM backgrounds are varied to working points corresponding to 80% and 95% background rejection to gauge the sensitivity of the analysis to these selections. This variation results in an uncertainty of up to 1.5% in the 70–90% centrality range but is negligible elsewhere. For the measurement of the p_T spectrum, this results in a 4% uncertainty in the lowest p_T bin but is small for higher p_T bins. Uncertainties related to MC-based backgrounds are negligible.

Both decay channels are combined into a single measurement using the best linear unbiased estimation method [41]. Correlations between channels resulting from the centrality calibration, N_{MB}, T_{AA}, and the acceptance correction are accounted for. In all cases the measurements from each channel are within 1.5 standard deviations (σ) of each other.

The Z boson v_2 as a function of PbPb centrality is shown in Fig. 1. A previous measurement from the ATLAS Collaboration at $\sqrt{s_{NN}} = 2.76$ TeV is also shown [5]. The new measurement in the 0–90% range is compatible with zero and is significantly more precise than the previous measurement. This finding reaffirms the expectation that Z bosons are produced early in a collision and are largely unaffected by final-state effects such as hydrodynamic flow and jet quenching.

The differential cross section of Z bosons as a function of $|y|$ for 0–100% events is shown in Fig. 2. Predictions from the aMC@NLO MC generator [19] interfaced with the CT14 free proton PDF [22], as well as the CT14+EPPS16 [21] and nCTEQ15 [42] nPDF sets are also shown. The models have been scaled by the 0-100% $T_{AA}\sigma_{MB}^{PbPb}$ value to account for increased production in PbPb collisions. The two nPDF sets do not significantly differ from each other, and both of them are compatible with the data. Differential cross sections as a function of p_T are shown in Fig. 3. The p_T distribution peaks around 5 GeV before sharply falling. Comparisons to the same aMC@NLO model with different (n)PDF sets are also shown. Although the general trend
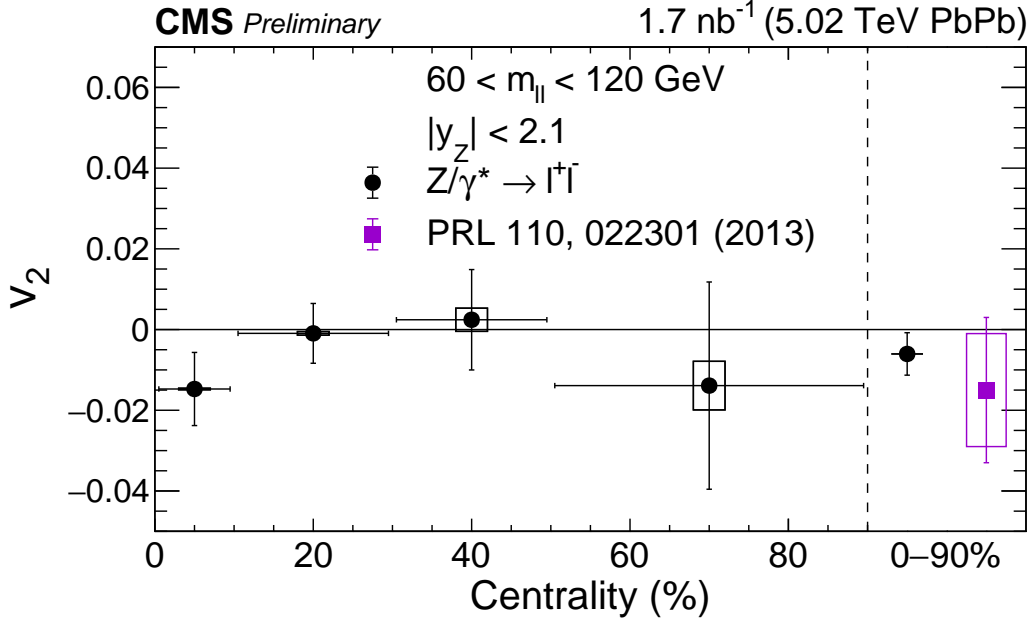
Figure 1: The v_2 of Z bosons in PbPb collisions for various centrality bins. The error bars represent statistical uncertainties, while the boxes represent systematic uncertainties. A previous measurement by the ATLAS Collaboration at $\sqrt{s_{NN}} = 2.76\,\text{TeV}$ is also shown [5].
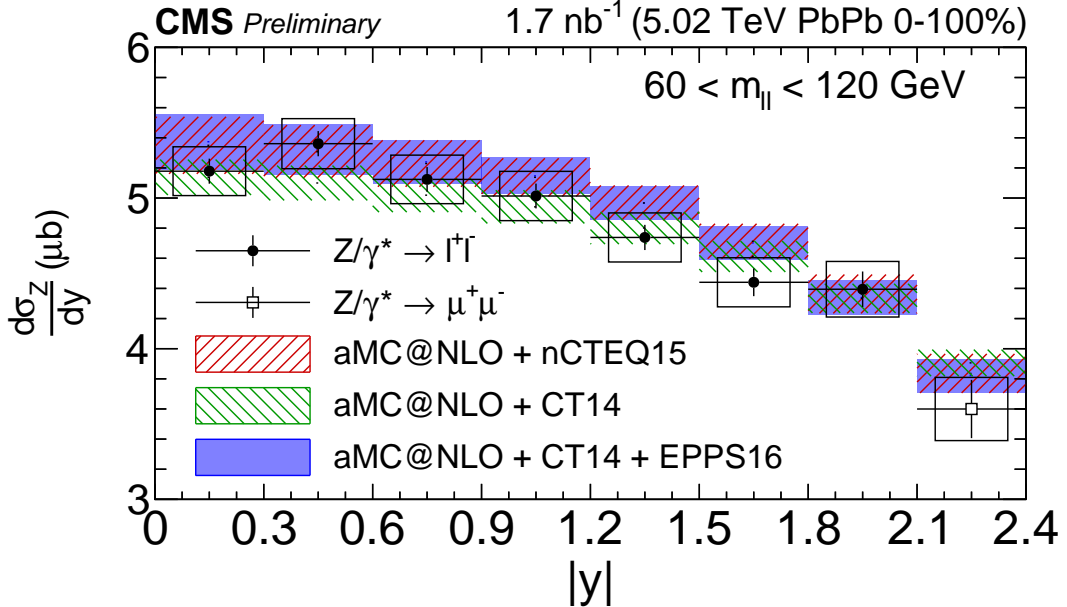

Figure 2: The Z boson differential cross section as a function of $|y|$. The error bars represent statistical uncertainties, while the boxes represent systematic uncertainties. Predictions using one PDF and two nPDF sets are also shown. The width of the model bands represents the contribution from PDF uncertainties, as well as the T_{AA} uncertainty.
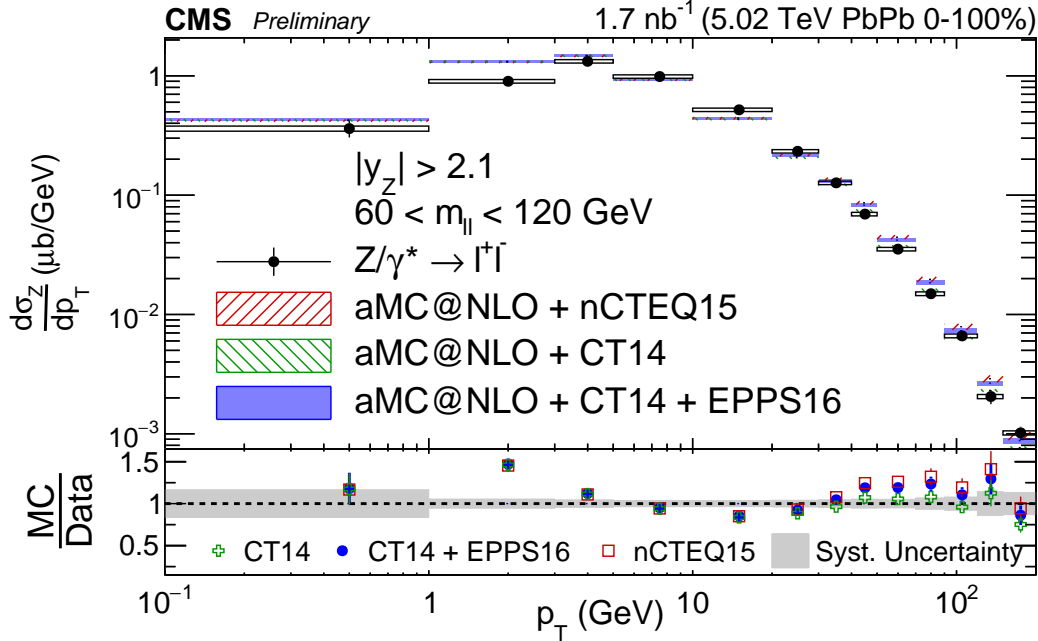
Figure 3: The Z boson differential cross section as a function of p_T. The error bars represent statistical uncertainties, while the boxes represent systematic uncertainties. Predictions using one PDF and two nPDF sets are also shown. The bottom panel shows a ratio of the predictions to data. The width of the model bands represents the contribution from PDF uncertainties, as well as the T_{AA} uncertainty.

of the data is correctly reproduced by the MC, some discrepancy is observed. The different (n)PDF sets do not differ at low p_T, but a slight splitting of $\approx 10\%$ can be seen for $p_T > 50\,\text{GeV}$. In this kinematic region, contributions involving the scattering of an initial-state gluon cause the spectrum to be sensitive to the gluon nPDF. Studies in MC indicate that the Bjorken x of the gluon tends to be in the antishadowing kinematic region [43], where CT14+EPPS16 and nCTEQ15 differ by up to 20%. Thus, the high p_T Z boson spectrum could potentially be used to constrain the gluon nPDF. However, the differences between the two nPDF sets are still smaller than the overall deviation of the MC model from the data, indicating that improvements in the modeling of the overall spectrum might be needed before considering nPDF modifications.

The T_{AA}-scaled Z boson yields are shown in Fig. 4 as a function of centrality. The $Z \to \ell\ell$ cross section per binary nucleon-nucleon collision (σ_{NN}^Z) after accounting for isospin and nPDF effects is shown by the dashed line. This quantity is calculated using the aMC@NLO MC generator [19] and the CT14+EPPS16 nPDF set [21, 22]. The 0–90% measurement is consistent with this cross section. The measurements for centralities less than 40% are also compatible with it, indicating that the N_{coll} scaling assumption works well for Z bosons in central events. This is consistent with the conclusions from previous analyses of Z boson production [4–6]. However, a decreasing trend for the 40–90% centrality range can be seen, which was not observed with less precise measurements. The significance of this deviation from σ_{NN}^Z is 2.1σ (2.8σ) in the 40–90% (70–90%) range. This effect is not expected to be caused by a quenching effect, which would be present in more central events. Additionally, any centrality-dependent modification caused by nPDF effects is expected to be smaller.

One potential explanation for this trend is the presence of initial state geometry and centrality selection biases in these peripheral events [44]. Initial state geometry biases can arise because
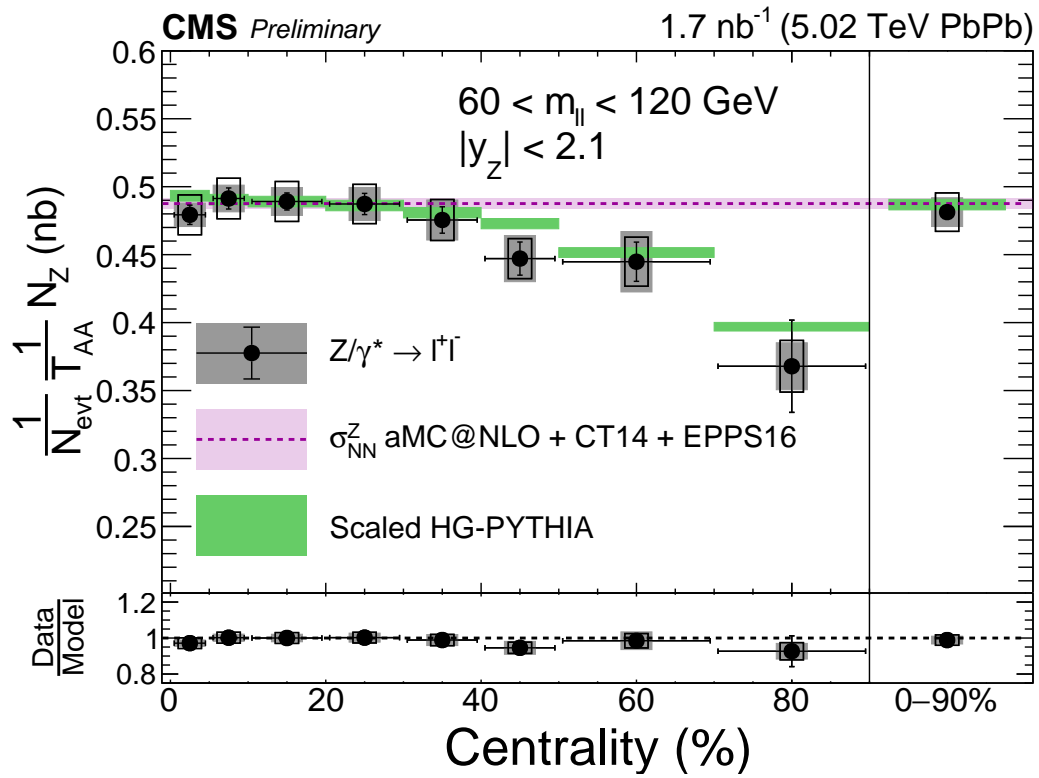
Figure 4: The T_{AA}-scaled yields of Z bosons as a function of centrality. The error bars, hollow boxes, and solid gray boxes represent the statistical, systematic, and T_{AA} uncertainties, respectively. The value of σ_{NN}^Z and the HG-PYTHIA model are shown for comparison, with the width of the bands representing nPDF uncertainties.

bound nucleons have a spatial distribution which can bias the average nucleon-nucleon impact parameter away from that of pp collisions. Likewise, correlations between hard processes and the soft particle production used for estimating centrality can bias the average N_{coll} in a given centrality range away from the Glauber expectation. Such effects have already been studied in the context of charged-hadron production by the ALICE and CMS Collaborations [45, 46]. The HG-PYTHIA model [44] attempts to describe these geometric and selection biases by using the HIJING [47] event generator to simulate the initial geometry of a heavy ion event. The particle production is then modeled by overlaying a PYTHIA 8 (v2.4.3) [23] event for each nucleon-nucleon scattering. These "heavy ion" MC events contain no physics related to the QGP. To compare this model to the data, the nuclear modification factor for hard scatterings was calculated and scaled by σ_{NN}^{Z}. This can be seen by the green boxes on Fig. 4, which are consistent with the data. This indicates that the downward trend in peripheral events can be largely explained by a combination of geometric and selection biases. The result is somewhat different from recent results from the ATLAS Collaboration comparing the yields of Z and W bosons to HG-PYTHIA, which indicated that the model did not seem to describe the data [6].

As uncertainties on the measurement are comparable to the Glauber uncertainties, the quantity $N_{\text{Z}}/(\sigma_{\text{NN}}^{Z} N_{\text{evt}})$ provides a new data-driven proxy for T_{AA}. This would eliminate the need for the Glauber modeling and the related assumptions about nuclear structure that are needed as its inputs. Furthermore, such a quantity would have potential centrality and selection biases built in, allowing for cancellation of these effects when measuring quantities such as the nuclear modification factor. Such cancellations are crucial for studies of the onset of jet quenching in peripheral collisions and other systems like pp and pPb.

In summary, high precision Z boson yields and elliptic flow coefficient (v_2) have been measured as a function of centrality in lead-lead collisions at a center-of-mass energy per nucleon-nucleon pair of 5.02 TeV. The Z boson v_2 is compatible with zero, consistent with the expectation of no significant final-state modifications experienced by Z bosons from the presence of a quark-gluon plasma. The differential cross section of Z bosons is found to agree with a model including two different nuclear parton distributions as a function of rapidity. However, some discrepancies are observed as a function of transverse momentum. Appropriately scaled Z boson yields have a flat trend as a function of centrality in the 0–40% range. A decreasing trend is seen for the first time toward more peripheral events. This trend is compatible with the HG-PYTHIA model which considers initial collision geometry and centrality selection biases. Results presented in this note provide a new data-driven proxy for estimating the average nucleon-nucleon luminosity of a heavy ion collision. This quantity could avoid uncertainties in Glauber modeling and account for potential biases related to event selection and centrality calibration. Such a method paves the way for searching for the onset of hot medium effects on colored hard probes in peripheral and small-system collision events in the future.

References

[1] J. Bjorken, "Energy Loss of Energetic Partons in Quark - Gluon Plasma: Possible Extinction of High p_{T} Jets in Hadron - Hadron Collisions", Technical Report FERMILAB-PUB-82-059-T, 1982.

[2] D. d'Enterria, "Jet quenching", *Landolt-Bornstein* **23** (2010) 471, `doi:10.1007/978-3-642-01539-7_16, arXiv:0902.2011`.

[3] M. L. Miller, K. Reygers, S. J. Sanders, and P. Steinberg, "Glauber modeling in high energy nuclear collisions", *Ann. Rev. Nucl. Part. Sci.* **57** (2007) 205,

`doi:10.1146/annurev.nucl.57.090506.123020, arXiv:nucl-ex/0701025.`

[4] CMS Collaboration, "Study of Z production in PbPb and pp collisions at $\sqrt{s_{NN}} = 2.76$ TeV in the dimuon and dielectron decay channels", *JHEP* **03** (2015) 022, `doi:10.1007/JHEP03(2015)022, arXiv:1410.4825.`

[5] ATLAS Collaboration, "Measurement of Z boson Production in Pb+Pb Collisions at $\sqrt{s_{NN}} = 2.76$ TeV with the ATLAS Detector", *Phys. Rev. Lett.* **110** (2013) 022301, `doi:10.1103/PhysRevLett.110.022301, arXiv:1210.6486.`

[6] ATLAS Collaboration, "Z boson production in Pb+Pb collisions at $\sqrt{s_{NN}}= 5.02$ TeV measured by the ATLAS experiment", *Phys. Lett. B* **802** (2020) 135262, `doi:10.1016/j.physletb.2020.135262, arXiv:1910.13396.`

[7] ALICE Collaboration, "Z-boson production in p-Pb collisions at $\sqrt{s_{NN}} = 8.16$ TeV and Pb-Pb collisions at $\sqrt{s_{NN}} = 5.02$ TeV", `arXiv:2005.11126.`

[8] ATLAS Collaboration, "Measurement of $W^{\pm}$ boson production in Pb+Pb collisions at $\sqrt{s_{NN}} = 5.02$ TeV with the ATLAS detector", *Eur. Phys. J. C* **79** (2019) 935, `doi:10.1140/epjc/s10052-019-7439-3, arXiv:1907.10414.`

[9] CMS Collaboration, "Study of W boson production in PbPb and *pp* collisions at $\sqrt{s_{NN}} = 2.76$ TeV", *Phys. Lett. B* **715** (2012) 66, `doi:10.1016/j.physletb.2012.07.025, arXiv:1205.6334.`

[10] ALICE Collaboration, "Direct photon production in Pb-Pb collisions at $\sqrt{s_{NN}} = 2.76$ TeV", *Phys. Lett. B* **754** (2016) 235, `doi:10.1016/j.physletb.2016.01.020,` `arXiv:1509.07324.`

[11] ATLAS Collaboration, "Centrality, rapidity and transverse momentum dependence of isolated prompt photon production in lead-lead collisions at $\sqrt{s_{NN}} = 2.76$ TeV measured with the ATLAS detector", *Phys. Rev. C* **93** (2016) 034914, `doi:10.1103/PhysRevC.93.034914, arXiv:1506.08552.`

[12] CMS Collaboration, "Measurement of isolated photon production in *pp* and PbPb collisions at $\sqrt{s_{NN}} = 2.76$ TeV", *Phys. Lett. B* **710** (2012) 256, `doi:10.1016/j.physletb.2012.02.077, arXiv:1201.3093.`

[13] K. Dusling, W. Li, and B. Schenke, "Novel collective phenomena in high-energy proton-proton and proton-nucleus collisions", *Int. J. Mod. Phys. E* **25** (2016) 1630002, `doi:10.1142/S0218301316300022, arXiv:1509.07939.`

[14] J. L. Nagle and W. A. Zajc, "Small System Collectivity in Relativistic Hadronic and Nuclear Collisions", *Ann. Rev. Nucl. Part. Sci.* **68** (2018) 211, `doi:10.1146/annurev-nucl-101916-123209, arXiv:1801.03477.`

[15] M. Luzum and J.-Y. Ollitrault, "Eliminating experimental bias in anisotropic-flow measurements of high-energy nuclear collisions", *Phys. Rev. C* **87** (2013) 044907, `doi:10.1103/PhysRevC.87.044907, arXiv:1209.2323.`

[16] CMS Collaboration, "The CMS trigger system", *JINST* **12** (2017) P01020, `doi:10.1088/1748-0221/12/01/P01020, arXiv:1609.02366.`

[17] CMS Collaboration, "The CMS experiment at the CERN LHC", *JINST* **3** (2008) S08004, `doi:10.1088/1748-0221/3/08/S08004.`

[18] C. Loizides, J. Kamin, and D. d'Enterria, "Improved Monte Carlo Glauber predictions at present and future nuclear colliders", *Phys. Rev. C* **97** (2018) 054910, `doi:10.1103/PhysRevC.97.054910`, `arXiv:1710.07098`. [erratum: Phys. Rev. C 99 (2019) 019901].

[19] J. Alwall et al., "The automated computation of tree-level and next-to-leading order differential cross sections, and their matching to parton shower simulations", *JHEP* **07** (2014) 079, `doi:10.1007/JHEP07(2014)079`, `arXiv:1405.0301`.

[20] R. Frederix and S. Frixione, "Merging meets matching in MC@NLO", *JHEP* **12** (2012) 061, `doi:10.1007/JHEP12(2012)061`, `arXiv:1209.6215`.

[21] K. J. Eskola, P. Paakkinen, H. Paukkunen, and C. A. Salgado, "EPPS16: Nuclear parton distributions with LHC data", *Eur. Phys. J. C* **77** (2017) 163, `doi:10.1140/epjc/s10052-017-4725-9`, `arXiv:1612.05741`.

[22] S. Dulat et al., "New parton distribution functions from a global analysis of quantum chromodynamics", *Phys. Rev. D* **93** (2016) 033006, `doi:10.1103/PhysRevD.93.033006`, `arXiv:1506.07443`.

[23] T. Sjostrand, S. Mrenna, and P. Z. Skands, "A Brief Introduction to PYTHIA 8.1", *Comput. Phys. Commun.* **178** (2008) 852, `doi:10.1016/j.cpc.2008.01.036`, `arXiv:0710.3820`.

[24] T. Sjostrand et al., "An Introduction to PYTHIA 8.2", *Comput. Phys. Commun.* **191** (2015) 159, `doi:10.1016/j.cpc.2015.01.024`, `arXiv:1410.3012`.

[25] CMS Collaboration, "Extraction and validation of a new set of CMS PYTHIA8 tunes from underlying-event measurements", `arXiv:1903.12179`.

[26] I. P. Lokhtin and A. M. Snigirev, "A Model of jet quenching in ultrarelativistic heavy ion collisions and high-p(T) hadron spectra at RHIC", *Eur. Phys. J. C* **45** (2006) 211, `doi:10.1140/epjc/s2005-02426-3`, `arXiv:hep-ph/0506189`.

[27] GEANT4 Collaboration, "GEANT4: A Simulation toolkit", *Nucl. Instrum. Meth. A* **506** (2003) 250, `doi:10.1016/S0168-9002(03)01368-8`.

[28] CMS Collaboration, "Particle-flow reconstruction and global event description with the CMS detector", *JINST* **12** (2017) P10003, `doi:10.1088/1748-0221/12/10/P10003`, `arXiv:1706.04965`.

[29] CMS Collaboration, "Performance of the CMS muon detector and muon reconstruction with proton-proton collisions at $\sqrt{s} = 13$ TeV", *JINST* **13** (2018) P06015, `doi:10.1088/1748-0221/13/06/P06015`, `arXiv:1804.04528`.

[30] CMS Collaboration, "Performance of Electron Reconstruction and Selection with the CMS Detector in Proton-Proton Collisions at $\sqrt{s} = 8$ TeV", *JINST* **10** (2015) P06005, `doi:10.1088/1748-0221/10/06/P06005`, `arXiv:1502.02701`.

[31] A. Hocker et al., "TMVA - Toolkit for Multivariate Data Analysis", `arXiv:physics/0703039`.

[32] CMS Collaboration, "Measurements of Inclusive *W* and *Z* Cross Sections in *pp* Collisions at $\sqrt{s} = 7$ TeV", *JHEP* **01** (2011) 080, `doi:10.1007/JHEP01(2011)080`, `arXiv:1012.2466`.

[33] Particle Data Group Collaboration, "Review of particle physics", *Phys. Rev. D* **98** (2018) 030001, `doi:10.1103/PhysRevD.98.030001`.

[34] CMS Collaboration, "Evidence for light-by-light scattering and searches for axion-like particles in ultraperipheral PbPb collisions at $\sqrt{s_{NN}}$ = 5.02 TeV", *Phys. Lett. B* **797** (2019) 134826, `doi:10.1016/j.physletb.2019.134826`, `arXiv:1810.04602`.

[35] S. R. Klein et al., "STARlight: A Monte Carlo simulation program for ultra-peripheral collisions of relativistic ions", *Comput. Phys. Commun.* **212** (2017) 258, `doi:10.1016/j.cpc.2016.10.016`, `arXiv:1607.03838`.

[36] T. Adye, "Unfolding algorithms and tests using RooUnfold", in *Proceedings, PHYSTAT 2011 Workshop on Statistical Issues Related to Discovery Claims in Search Experiments and Unfolding, CERN,Geneva, Switzerland 17-20 January 2011*, p. 313, CERN. CERN, Geneva, 2011. `arXiv:1105.1160`. `doi:10.5170/CERN-2011-006.313`.

[37] CMS Collaboration, "Measurement of prompt D^0 meson azimuthal anisotropy in Pb-Pb collisions at $\sqrt{s_{NN}}$ = 5.02 TeV", *Phys. Rev. Lett.* **120** (2018) 202301, `doi:10.1103/PhysRevLett.120.202301`, `arXiv:1708.03497`.

[38] A. M. Poskanzer and S. A. Voloshin, "Methods for analyzing anisotropic flow in relativistic nuclear collisions", *Phys. Rev. C* **58** (1998) 1671, `doi:10.1103/PhysRevC.58.1671`, `arXiv:nucl-ex/9805001`.

[39] NA49 Collaboration, "Directed and elliptic flow of charged pions and protons in Pb + Pb collisions at 40-A-GeV and 158-A-GeV", *Phys. Rev. C* **68** (2003) 034903, `doi:10.1103/PhysRevC.68.034903`, `arXiv:nucl-ex/0303001`.

[40] J. Butterworth et al., "PDF4LHC recommendations for LHC Run II", *J. Phys. G* **43** (2016) 023001, `doi:10.1088/0954-3899/43/2/023001`, `arXiv:1510.03865`.

[41] A. Valassi, "Combining correlated measurements of several different physical quantities", *Nucl. Instrum. Meth. A* **500** (2003) 391, `doi:10.1016/S0168-9002(03)00329-2`.

[42] K. Kovarik et al., "nCTEQ15 - Global analysis of nuclear parton distributions with uncertainties in the CTEQ framework", *Phys. Rev. D* **93** (2016) 085037, `doi:10.1103/PhysRevD.93.085037`, `arXiv:1509.00792`.

[43] H. Paukkunen, "Nuclear PDFs in the beginning of the LHC era", *Nucl. Phys. A* **926** (2014) 24, `doi:10.1016/j.nuclphysa.2014.04.001`, `arXiv:1401.2345`.

[44] C. Loizides and A. Morsch, "Absence of jet quenching in peripheral nucleusnucleus collisions", *Phys. Lett. B* **773** (2017) 408, `doi:10.1016/j.physletb.2017.09.002`, `arXiv:1705.08856`.

[45] CMS Collaboration, "Charged-particle nuclear modification factors in XeXe collisions at $\sqrt{s_{NN}}$ = 5.44 TeV", *JHEP* **10** (2018) 138, `doi:10.1007/JHEP10(2018)138`, `arXiv:1809.00201`.

[46] ALICE Collaboration, "Analysis of the apparent nuclear modification in peripheral Pb-Pb collisions at 5.02 TeV", *Phys. Lett. B* **793** (2019) 420, `doi:10.1016/j.physletb.2019.04.047`, `arXiv:1805.05212`.

[47] M. Gyulassy and X.-N. Wang, "HIJING 1.0: A Monte Carlo program for parton and particle production in high-energy hadronic and nuclear collisions", *Comput. Phys. Commun.* **83** (1994) 307, `doi:10.1016/0010-4655(94)90057-4`, `arXiv:nucl-th/9502021`.